Remote Sensing of Environment 119 (2012) 255–265

Contents lists available at SciVerse ScienceDirect

Remote Sensing of Environment

journal homepage: www.elsevier.com/locate/rse

A general Landsat model to predict canopy defoliation in broadleaf deciduous forests

Philip A. Townsend [a,*], Aditya Singh [a], Jane R. Foster [a], Nathan J. Rehberg [a], Clayton C. Kingdon [a], Keith N. Eshleman [b], Steven W. Seagle [c]

[a] University of Wisconsin-Madison, Department of Forest and Wildlife Ecology, 1630 Linden Drive, Madison, WI 53706, United States
[b] University of Maryland Center for Environmental Science, Appalachian Laboratory, 301 Braddock Road, Frostburg, MD 21532, United States
[c] Appalachian State University, Department of Biology, 572 Rivers Street, Boone, NC 28608, United States

ARTICLE INFO

Article history:
Received 8 March 2011
Received in revised form 29 December 2011
Accepted 30 December 2011
Available online 26 January 2012

Keywords:
Defoliation
Landsat
NDII
Gypsy moth
Change detection

ABSTRACT

Defoliation by insect herbivores can be a persistent disturbance affecting ecosystem functioning. We developed an approach to map canopy defoliation due to gypsy moth based on site differences in Landsat vegetation index values between non-defoliation and defoliation dates. Using field data from two study areas in the U.S. central Appalachians and five different years (2000, 2001, 2006, 2007, and 2008), we fit a sigmoidal model predicting defoliation as a function of the difference in the vegetation index. We found that the normalized difference infrared index (NDII, [Band 4 − Band 5]/[Band 4 + Band 5]) and the moisture stress index (Band 5/Band 4) worked better than visible-near infrared indices such as NDVI for mapping defoliation. We report a global 2-term fixed-effects model using all years that was at least as good as a mixed-effects model that varied the model coefficients by year. The final model was: proportion of foliage retained $= 1/(1+\exp(3.057 - 31.483 * [\mathrm{NDII}_{\mathrm{base\ year}} - \mathrm{NDII}_{\mathrm{disturbance\ year}}])$. Cross-validation by dropping each year of data and subsequently refitting the remaining data generated an RMS error estimate of 14.9% defoliation, a mean absolute error of 10.8% and a cross-validation R^2 of 0.805. The results show that a robust, general model of percent defoliation can be developed to make continuous rather than categorical maps of defoliation across years and study sites based on field data collected using different sampling methods.

1. Introduction

Temperate forests throughout the world experience periodic infestations by herbivorous insects. The damage to forests can be extensive. Dale et al. (2001) concluded that insects and pathogens are the most expensive disturbance agents in North America, affecting 20 M ha in the U.S. per year. Among insects and pathogens, defoliators are herbivores that consume leaves but do not necessarily kill trees. Defoliation by herbivores accounts for 5–10 M ha of disturbance per year in the U.S., of which 0.5–1 M ha on average and over 5 M ha in peak years are attributable to the gypsy moth (*Lymantria dispar* L.; Man, 2010). Defoliation events may not result in widespread mortality, but herbivory does reduce tree growth (Katovich & Hanson, 2001; Muzika & Liebhold, 1999; Naidoo & Lechowicz, 2001) and can kill trees after successive years of defoliation (Conway et al., 1999; Fajvan & Wood, 1996). In addition, several studies have shown significant effects on forest nutrient cycling following defoliation events, for example increases in nitrogen export from forested watersheds (Eshleman et al., 1998; Swank et al., 1981; Townsend et al., 2004). In eastern North America, the chief defoliating insects are the exotic gypsy moth and native forest tent caterpillar, spruce budworm and jack pine budworm. Of these species, larvae of the gypsy moth (caterpillars) defoliate the largest area, and because it is a non-native species whose range is expanding, the gypsy moth is of considerable research and management interest. In this paper, we focus on defoliation of Appalachian oak forests by the gypsy moth, but demonstrate an application of our approach to defoliation by the forest tent caterpillar of Minnesota aspen forests.

Starting with Landsat, satellite-based remote sensing has long been used to detect defoliation by herbivores, including the gypsy moth on deciduous broadleaf forests (Ciesla et al., 1989; Hurley et al., 2004; Joria & Ahearn, 1991; Muchoney and Haack, 1994; Williams et al., 1985), several defoliators of aspen forests (Hall et al., 2003; Moskal & Franklin, 2004), and the jack pine budworm (Radeloff et al., 1999), pine sawfly (Eklundh et al., 2009), and spruce budworm (Franklin et al., 2008) in evergreen conifers. Numerous approaches have been demonstrated, including classification (Muchoney & Haack, 1994; Spruce et al., 2011), unmixing (Radeloff et al., 1999), image algebra (Hurley et al., 2004; Muchoney & Haack, 1994; Royle & Lathrop, 1997), vegetation indices (de Beurs & Townsend, 2008), thresholds (Eklundh et al., 2009; Spruce et al., 2011) and change vector analysis (Townsend et al., 2004). Landsat data have been used most widely, but studies have shown the capacity of a wide range of sensors, including SPOT (Ciesla et al., 1989; Joria & Ahearn, 1991) and MODIS (de Beurs & Townsend, 2008; Eklundh et al., 2009; Spruce et al., 2011). In our review of the literature, almost all efforts to

* Corresponding author. Tel.: +1 608 262 1669.
E-mail address: ptownsend@wisc.edu (P.A. Townsend).

0034-4257/$ – see front matter © 2012 Elsevier Inc. All rights reserved.
doi:10.1016/j.rse.2011.12.023

map defoliation have yielded maps that are either binary (i.e., defoliated or not, e.g., Spruce et al., 2011) or with a small number of general categories (e.g., moderate, heavy defoliation). Alternative to satellite remote sensing, aerial disturbance detection sketch maps generated by the US Forest service (FHTET Geoportal, http://svinetfc8.fs.fed.us/aerialsurvey/, accessed 27 January 2011) are useful for broad-scale monitoring, but are often inconsistent in detail and spatial coverage (Johnson & Ross, 2008; MacLean & MacKinnon, 1996) as discussed in detail by de Beurs and Townsend (2008). These efforts show the potential of satellite and aerial methods for detecting insect-induced defoliation, though none of the products previous to this project provide percent estimates of forest defoliation. In this paper, we demonstrate a method to map defoliation as a continuous measure of proportion defoliated.

Mapping of defoliation has employed a wide range of vegetation indices, including measures that exploit the red/near infrared (NIR) contrast such as NDVI and WDRVI (Eklundh et al., 2009; Hurley et al., 2004; Jepsen et al., 2009), the tasseled cap indices (Townsend et al., 2004), and indices that are responsive to vegetation moisture stress based on the contrast between NIR and shortwave infrared (SWIR) reflectance (Fraser & Latifovic, 2005; Vogelmann & Rock, 1989). In this paper, we evaluate some common indices for their ability to distinguish the intensity of gypsy moth defoliation.

Mapping of defoliation can be more challenging than mapping mortality due to wood-boring beetles such as the mountain pine beetle because defoliation is an ephemeral process. Trees can re-foliate, often during the same season, as in broadleaf hardwoods, or over the course of the following year, as with conifers. A few studies have taken advantage of this to distinguish defoliation from other disturbances by looking at trends in vegetation indices over a single season (de Beurs & Townsend, 2008; Hurley et al., 2004), but from a practical standpoint, this approach cannot be routinely applied in temperate regions because of cloud-cover at crucial times of insect activity. As an alternative approach, studies have used anniversary-date change detection to map defoliation; reflectance measurements from disturbed and undisturbed years are employed to discriminate transient changes in forest canopies. We chose this approach, as it offers the maximum flexibility for detecting repeat defoliations in areas where summer cloud cover is an issue. Although the ideal timing for image acquisition is just past the completion of defoliation (e.g. at pupation for caterpillars), we also examine how variation in the timing of image acquisition affects mapping of defoliation intensity for the observed years within the 2000–2008 timeframe.

2. Methods

2.1. Study area

We examined two outbreaks of gypsy moth defoliation in two predominantly-oak forested study areas (collectively 50,000 ha) located in the central Appalachian ecoregion (USA) (Fig. 1). We collected data during a 2000–2001 outbreak in the Green Ridge (GR) area that covers parts of western Maryland, south central Pennsylvania and the eastern panhandle of West Virginia; comparable data were collected during a 2006–2008 outbreak in the Savage River (SR) area in far western Maryland. Although the two study areas are less than 100 km apart, they differ considerably in climate, with Green Ridge being in the comparatively warmer Ridge and Valley physiographic province (means: monthly temperature −1.0 to 23.6 °C, annual precipitation 1023 mm) and Savage River in the cooler, wetter Appalachian Plateau (means: monthly temperature −3.2 to 20.9 °C, annual precipitation 1216 mm) (Townsend et al., 2004). The growing season initiates 2–3 weeks sooner in GR than SR. Forests of both study areas are dominated by oaks. The study areas have experienced several waves of gypsy moth defoliation, including 1983–1984, 1987, 1990–1991 and 2000–2001 in GR and 1986–1987, 1990–1991, and 2006–2008 in SR. As a test of the generality of our method, we also applied our results to a 40,000-ha aspen-dominated study area in northern Minnesota that was affected by the forest tent caterpillar in 2001.

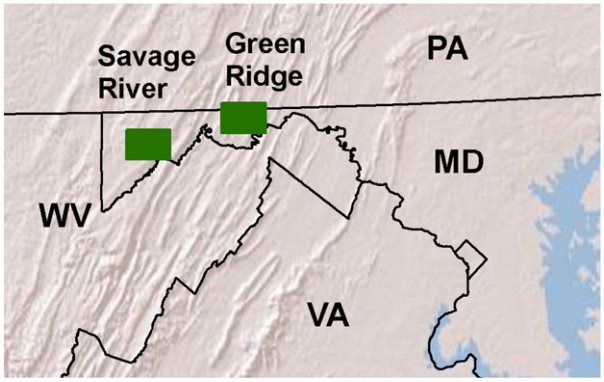

Fig. 1. Study area in western Maryland and adjacent Pennsylvania and West Virginia. Boxes indicate areas shown in Figs. 2 and 5. Study areas are each 28 km wide.

2.2. Field data

53 field plots were located within the gypsy moth study areas. Field plots consisted of two crossing 60×60 m transects defining five subplots (the intersection and each end of the X) at which tree composition was characterized using the variable plot-size method (metric basal area factor 2 prism) described by Townsend (2001). This plot design is optimized to ensure that the area on the ground captures at least one full Landsat 30 m pixel. Plot data included measurements of tree height, diameter at breast height (DBH) and basal area. From the tree data, we calculated total dry foliar biomass using the allometric equations in Jenkins et al. (2003).

Defoliation by the gypsy moth was characterized in two ways. In 2000, 2001, 2006, and 2007, we measured weekly frass-fall (excrement deposition) at each plot during the defoliation event using 4 or 5 litter traps with collection areas ranging from 1.32 to 2.63 m^2. Dried frass samples were converted to mass of foliage consumed (kg-ha^{-1}) based on a food use efficiency of 0.14 (W. Mattson, pers. comm.) and then to proportion defoliated by dividing foliage consumed by total foliar biomass. In 2006–2008, two technicians visually estimated defoliation weekly for 9–15 trees per plot in ten percent increments, from which we calculated seasonal maximum percent defoliation for each plot (weighting the estimate for each tree by its DBH). Both frass and visual estimates were available in 2006–2007 and were highly correlated (data not shown, Pearson's r correlation >0.9 for all years with both data sets); in the analyses presented here we used the measure of percent defoliation based on visual estimates because it was a more direct estimate of foliar removal than the frass data.

Our field sampling in Green Ridge resulted in data from 15 plots in 2000 and 12 different plots in 2001. 18 plots were also sampled in Green Ridge in 2008, although in the absence of significant gypsy moth defoliation, these plots were not used in the image analysis. In Savage River, we sampled the same 20 plots in 2006, 2007 and 2008. In 2007, the peak defoliation year, we sampled 6 additional plots (Table 1). The final analysis used 84 of the 93 samples, with 2 plots removed due to selective logging, 3 due to clouds or shadows, and four (from 2000) because of a secondary defoliation by phasmids ("walking sticks") that occurred in August and September of 1999, skewing base-year foliar estimates for these plots.

Table 1
Image data used in the study.

		Base			Defoliation			
Year	Study site	Date	Sensor	Path	Date	Sensor	Path	Description
2000	Green Ridge	8/4/1999	ETM+	16	8/22/2000	ETM+	16	11 plots
2001	Green Ridge	8/4/1999	ETM+	16	8/25/2001	ETM+	16	12 plots
2006	Savage River	7/7/2001	TM	17	8/6/2006	TM	17	20 plots
2007	Savage River	7/7/2001	TM	17	8/25/2007	TM	17	24 plots
2008	Savage River	7/7/2001	TM	17	7/19/2008	TM	16	17 plots
Model extension								
2002	Green Ridge	8/4/1999	ETM+	16	8/4/2002	ETM+	16	Non-defoliation year
2008	Green Ridge	7/30/2006	TM	16	8/20/2008	TM	16	Non-defoliation year
2001	NE Minnesota	6/9/1997	TM	26	6/12/2001	ETM+	26	Different defoliator

2.3. Remotely sensed imagery and vegetation indices

Image change detection was used to map proportional defoliation using one image from a non-defoliation year and an image from the defoliation year (Table 1). Image timing played a role in image selection, but because of persistent cloudiness in the Appalachian Mountains, we were generally limited to one relatively cloud-free post-June summer image per year. In our study areas, peak gypsy moth defoliation can vary from year to year due to inter-annual differences in weather, but usually occurs by late June or early July. Trees may begin to re-foliate 3–5 weeks following peak defoliation, with maximum re-foliation occurring by mid-August, depending on climate. Re-foliation is generally a fraction of total foliar biomass from an undisturbed year, and heavily defoliated stands may not re-foliate at all (see Fig. 3 in de Beurs & Townsend, 2008).

Although it has been suggested that the combination of pre-defoliation, peak defoliation, and post-defoliation images in the same year are most desirable for mapping gypsy moth defoliation (Hurley et al., 2004), this is not practical in montane forests where clouds can be frequent. Moreover, same-year pre-defoliation imagery is of limited value because the life cycle of the gypsy moth parallels spring green-up, with maximum defoliation occurring shortly after peak leaf expansion. We were concerned that post-defoliation re-foliation during a year would affect our analysis, and were fortunate that two post-defoliation images were available for the analysis of defoliation in 2001: 7/24/2001, just after peak defoliation, and 8/25/2001, when presumably any re-foliation would have occurred. We used the 25 August image for modeling because it was cloud-free, whereas the 24 July image was obscured by small cumulus clouds.

To develop a generalizable, repeatable method for mapping defoliation of broadleaf deciduous trees, we examined defoliation in five different years in two physiographically distinct study areas with different Landsat footprints. This approach required a repeatable method for image pre-processing and the use of easily-calculated image variables. We employed Landsat images downloaded from the USGS Global Visualization Viewer (www.glovis.gov). All images were processed identically: they were converted to top-of-atmosphere reflectance using coefficients provided in the image header data, then atmospherically corrected to percent reflectance following the LEDAPS atmospheric correction processing stream (Masek et al., 2006). LEDAPS employs the 6S radiative transfer code (Kotchenova et al., 2006) in conjunction with several atmospheric products to estimate Lambertian surface reflectance for each image pixel. Masek et al. (2006) report error rates of 0.5% absolute reflectance or 5% measured reflectance. We employed the C-factor topographic normalization technique of Teillet et al. (1982) to reduce the effects of differential illumination due to topography. Numerous alternative methods for atmospheric correction and topographic normalization are available for pre-processing multi-spectral imagery. Although it was outside the scope of our work to compare different techniques, we postulate that our approach will be applicable using other methods if they are applied uniformly and consistently to all images.

We tested ten different easily-computed Landsat vegetation indices for their capacity to detect defoliation (Table 2). These included indices that our previous work had shown to be effective for characterizing defoliation, including several indices that use the sensitivity of shortwave infrared (SWIR) reflectance to leaf water content and near infrared (NIR) reflectance to green vegetation biomass and hence, jointly, to vegetation stress. Undisturbed forests are expected to exhibit higher values of Normalized Difference Infrared Index (NDII) (Table 1, sometimes also referred to as the Normalized Difference Water Index (NDWI) or Normalized Difference Moisture Index (NDMI)) and lower values of MSI compared to defoliated forests due to the decline in water content from the loss of leaf area (de Beurs & Townsend, 2008). We also tested traditional indices such as NDVI and SVI because of their wide use for characterizing vegetation, as well as several others that other work by our group suggested may be sensitive to forest change (Wolter & Townsend, 2011; Wolter et al., 2008).

We did not employ several indices that we have previously used to characterize the relationship between forest disturbance and water quality in our study area, including the Tasseled Cap (Wetness and Greenness indices, Crist & Kauth, 1986; used in Townsend et al., 2004), the forest disturbance index of Healy et al. (2005, used in Eshleman et al., 2009 and Deel et al., accepted for publication) and a variety of modified vegetation indices such as the enhanced vegetation index (EVI, Huete et al., 2002). Many of these indices are strongly correlated with indices we used (e.g., see Jin & Sader, 2005), or require within-scene calibration to that limits the generality of the

Table 2
Landsat vegetation indices tested in the study.

Acronym	Name and equation for Landsat TM and ETM+	Reference[a]
AI	Autumn Index, TM3/TM1	Wolter and Townsend (2011)**
MIR	Middle Infrared Index, TM5/TM7	Elvidge and Lyon (1985)
MSI	Moisture Stress Index, TM5/TM4	Rock et al. (1986)
NDII5	Normalized Difference Infrared Index (Band 5), (TM4−TM5)/(TM4+TM5)	Hardisky et al. (1983)
NDII7	Normalized Difference Infrared Index (Band 7), (TM4−TM7)/(TM4+TM7)	Hunt and Rock (1989)
NDVI	Normalized Difference Vegetation Index (TM4−TM3)/(TM4+TM3)	Tucker (1979)
RA	Reflectance Absorption Index, TM4/(TM3+TM5)	Arzani and King (1997)
SVI	Simple NIR/RED Ratio, TM4/TM3	Jordan (1969)
SVR5	Shortwave to Visible Ratio (Band 5), 3*TM5/(TM1+TM2+TM3)	Wolter et al. (2008)
SVR7	Shortwave to Visible Ratio (Band 7), 3*TM7/(TM1+TM2+TM3)	Wolter et al. (2008)

[a] Many of these indices may have multiple appropriate citations.

index (such as the Healy et al. index). We make one radiometric modification to our data based on the observation that vegetation indices for closed-canopy undisturbed forests saturate at a uniform maximum VI. As such, we aligned our VI images by the eightieth percentile value of the distribution for forests in the whole VI image.

2.4. Statistical analyses

All statistical analyses employ proportion of foliage remaining (1 minus proportion defoliated) as the dependent variable, expressed as a range from 0 (completely defoliated) to 1 (no defoliation). We fit a negative logistic (sigmoidal) curve to predict the proportion of foliage remaining as a function of the change in a vegetation index between and a non-disturbance (base) year and the disturbance year, following:

$$\text{Foliage remaining(proportion)} = \frac{b}{1 + \exp[-(c + d * \Delta\text{VI})]}, \quad (1)$$

where the parameter b represents the asymptote (maximum foliage retained), c and d are parameters determining the shape of the sigmoidal curve, and ΔVI is the difference between years in the selected vegetation index (VI) for the plot, i.e.:

$$\Delta\text{VI} = \text{VI(base year)} - \text{VI(defoliation year)} \quad (2)$$

For all of the indices we tested except MSI, healthy green vegetation has a higher VI than damaged vegetation, so the expectation is that ΔVI increases as defoliation increases. Values of ΔVI close to zero or negative indicate stands with minimal disturbance between years. MSI, the ratio of Landsat band 5 to band 4, increases with decreasing vegetation vigor, so the form of the relationship is reversed. Our model (Eq. (1)) does not include an intercept, which would represent a lower bound to our estimate of the proportion of foliage retained. The lower bound is assumed to be zero, indicating complete defoliation. We did, however, model the upper asymptote, b, as all plots in our study exhibited some level of foliar damage due to herbivory.

Because we used data from five different years and two different study areas, we developed two forms of models, a global model, in which image VI is assumed to vary as a function of defoliation, independent of the year sampled. To address the possibility that the models differed between years, we also fit a mixed-effects model, in which a random effect (year) was fit for parameters c and d. Note that our prime interest was to develop the global model without random year effects, because it would be more generalizable to years not having field measurements. Defoliation and disturbance represent one component of change in the imagery, but some areas also experience increasing greenness. Although we did not directly sample forest regrowth, we calculated a measure of forest regrowth for 24 of our samples in Savage River that exhibited decreasing defoliation from 2006 or 2007 to later years. Regrowth is calculated as 1 + [defoliation in earlier year − defoliation in the later year] and effectively extends the range of measurements. We fit an alternative sigmoidal model to the defoliation plus regrowth data using Eq. (1).

We tested the 10 vegetation indices (Table 2) for their potential to characterize defoliation using the simplest form of Eq. (1), with $b = 1$ (asymptote of all foliage retained) and no random effects. The vegetation index exhibiting the best performance using the Akaike Information Criterion (AIC) and Schwartz's Bayes Information Criterion (BIC, see Burnham & Anderson, 2002) was then used for further model development, statistical testing and mapping. The traditional coefficient of determination (R^2) is not appropriate for non-linear models. As such, we report a generalized form of the coefficient of determination (Nagelkerke's pseudo-R^2) based on the likelihood function (Cox & Snell, 1989; Nagelkerke, 1991). However, AIC and BIC are generally considered better measures than R^2 for model selection because they penalize models with increasing complexity (i.e., more parameters). For evaluation of the models themselves, we report the mean absolute error of prediction (MAE) and root mean square error of prediction (RMSE). These measures are most useful for this work, as they provide measures of the level of expected error in units of proportion of the foliage remaining/consumed.

Preliminary efforts, including the results reported by de Beurs and Townsend (2008), indicated that vegetation indices using the near infrared (NIR) and shortwave infrared (SWIR) bands on Landsat were most sensitive to defoliation, so our expectation was that either NDII or MSI would be the preferred vegetation index. NDII has the benefit of being normalized, making numerical interpretation of differences between years relatively straightforward. In contrast, ΔMSI can potentially provide a wider dynamic range than NDII. Both indices reduce the effects of topography in imagery, although because it is normalized, NDII may be less sensitive to the effects of differences in illumination than MSI.

2.5. Model evaluation

We evaluated all predictive models using cross-validation by year. To do this, we dropped all data from each year successively and rebuilt the model using the remaining four years. We then applied the resulting model to the data from the dropped year and calculated cross-validation (CV) fit statistics, reported as CV-MAE, CV-RMSE and CV-R^2. As a secondary measure of cross-validation, we also report the model fit for each iterative model. Drastic changes in model performance for a particular dropped year, by either model improvement or decline, indicates that a particular year does not fit the overall trends in the relationship between defoliation and ΔVI.

Further testing of the predictive models involved map comparison and image substitution. We visually compared our maps of defoliation from each year to US Forest Service aerial sketch map data of gypsy moth defoliation. This provides no absolute validation of our results, as the sketch map data are discontinuous in spatial extent and, as reported elsewhere, are widely varying in overall quality (de Beurs & Townsend, 2008). However, they do provide a general qualitative measure of concurrence between our maps and an independent data source. We also applied our final model to images from years of known minimal defoliation (2002 in both areas, and 2008 in Green Ridge, based on sketch map data) to ensure that the model did not erroneously map defoliation where none occurred.

We were also interested in evaluating the importance of image date during the growing season for mapping defoliation. Because of the cloudiness of the Appalachian Mountain region, we were limited in the availability of relatively cloud-free images for this study, meaning that we employed images that were not optimally tied to peak defoliation. However, for 2001 and 2008, alternate images were available (Table 1). We applied the final model to the alternate images and compared these with the maps developed using the model data.

Finally, we hypothesized that in addition to being generalizable to gypsy moth defoliation in Appalachian forests, our model is sufficiently general to enable its application to defoliation by other herbivores of closed-canopy broadleaf deciduous forests. We therefore applied the model to a defoliation event by the forest tent caterpillar of aspen-dominated forests in the Arrowhead region of northeastern Minnesota. Such an approach facilitates the retrospective analysis of past forest disturbances for which field data are lacking, and represents the development of an index measure of defoliation (rather than a direct estimate), since calibration data are not available. For this analysis, we employed Landsat images for a defoliation year (2001) and a non-disturbance year (1997, see Table 1). The Minnesota Landsat images were processed identically to the Appalachian images.

3. Results

Indices that employed NIR and SWIR bands provided the best estimation of defoliation using the two-term fixed-effects ("global") model (Table 3). NDII5 and the closely related MSI produced nearly identical results, exhibiting a strong sigmoidal relationship between foliage retained and the change index (Fig. 3). The ability to detect defoliation using SWIR and NIR is clearly illustrated in pre- and post-defoliation Landsat images for the study area (Fig. 2). The cross-validation RMS error to predict foliage removal/retention as a function of ΔNDII5 was 14.9% with a cross-validation R^2 of 0.802. Average error on cross-validation was less than 11%. Indices employing visible wavelengths or exclusively SWIR bands performed less well, although the reflectance–absorption index (RA), which uses the sum of Landsat's red and 1.55–1.75 μm SWIR5 bands in the denominator, also performed well. NDII7, which uses the 2.08–2.35 μm SWIR7 channel, did not perform as well as NDII5, probably due to the lower signal in the SWIR7. NDVI performed less well than all of the SWIR/NIR-based indices (Fig. 3), with a much more scattered dispersion of points and several likely outliers. All years fall on the prediction line, with no apparent systematic bias by year.

For the remainder of the analyses we report ΔNDII5 exclusively. We tested whether our assumption of a "global" 2-term fixed-effects model (Table 4) based on a sigmoidal fit using all years of data was reasonable. We found that a mixed effects model using year as a random effect ($F_{(6,84)} = 148.9$, $p<0.001$) did not provide a statistically significant improvement over the global model. Although the mixed model was significant, the 95 percent confidence intervals for the random effects all bounded zero, indicating that they did not improve the model over a global fixed effects for parameters *c* and *d*. This interpretation is confirmed by the AIC for the two models, which was lower for the global model (−94.7 vs. −92.2), and generalized coefficient of determination, which was about the same for both models (0.844 vs. 0.842). The RMS error for the global model was slightly worse than for the mixed model (13.5% vs. 12.9%). The lower AIC and equivalent values of Nagelkerke's R^2 for the global model result from a lower model complexity (fewer parameters) compared to the mixed-effects model. Note that BIC was lower for the mixed effects model (−94.5) than the global model (−87.4), which does indicate that the mixed model is able to account for some of the variability in model fit across years.

Finally, we tested for the necessity of an upper asymptote for percent vegetation retained in the global model, by adding a third fixed parameter, *b*, which would represent a maximum amount of foliage retained, or conversely the minimum amount of defoliation measured. We performed this analysis because all plots – regardless of the presence of the gypsy moth – exhibited some measurable herbivory every year; there were no field plots with 100% foliage retained (Fig. 3). The results of this analysis also confirmed that the 2-parameter fixed effects model was sufficient. Model AIC was lower for the 2-parameter model (−94.7 vs. −92.8), RMS error was nearly identical (13.5% vs. 13.6%) and Nagelkerke's R^2 was the same (0.844). The estimated asymptote, *b*, for the 3-parameter model was 0.977 (or 97.7% foliage retained) with 95% confidence intervals of 0.873 and 1.081, indicating that a modeled asymptote does not differ measurably from the assumed asymptote of one in the model presented in Table 4. As such, all further results focus exclusively on the two-term global model to predict defoliation/retention using ΔNDII5.

We report the inflection point for the sigmoidal curves (Fig. 3) in Table 3. The inflection point indicates the value of ΔNDII5 at which point the model effectively separates the most defoliated and least defoliated observations. For ΔNDII5, this value is 0.068, so that an approximate decrease of 0.07 in NDII5 captures major defoliation. NDII values range −1 to +1, but are effectively much smaller than this (+0.28 to +0.52), so that a 0.07 change in NDII5 represents about 30% of the effective range of the index. We conclude that NDII5 is quite sensitive to differences in foliage present between defoliation

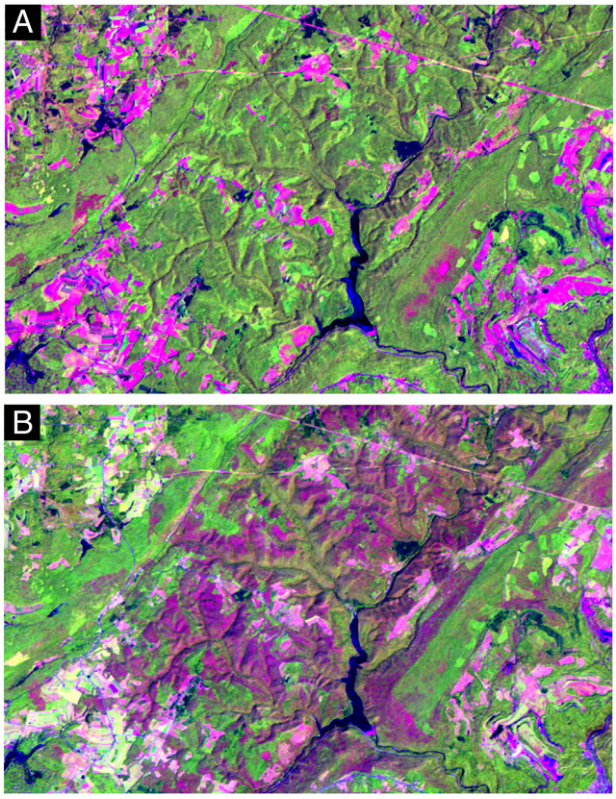

Fig. 2. False color images of the Savage River area for 7 July 2001 (top, not defoliated) and 25 August 2007 (bottom, defoliated). Band combination is Landsat channels 5, 4, and 3 in RGB. Study area is 28 km wide.

Table 3
Comparison of 2-term fixed-effects models for all indices. Index names listed in Table 2.

Index	Model diagnostics						Cross-validation results		
	AIC	BIC	MAE	RMSE	Inflection	N-RSQ	CV-MAE	CV-RMSE	CV-RSQ
NDII5	−94.7	−87.4	0.097	0.135	0.068	0.844	0.106	0.145	0.821
MSI	−88.5	−81.2	0.102	0.140	0.320	0.832	0.111	0.151	0.804
RA	−81.6	−74.3	0.108	0.146	−0.056	0.817	0.117	0.157	0.788
NDII7	−68.6	−61.4	0.112	0.158	0.067	0.787	0.120	0.169	0.756
NDVI	−53.1	−45.8	0.122	0.173	0.035	0.744	0.129	0.178	0.728
SVI	−2.3	5.0	0.182	0.235	4.732	0.531	0.205	0.262	0.414
MIR	−1.9	5.4	0.182	0.235	0.328	0.528	0.189	0.243	0.495
SVR	29.9	37.2	0.218	0.284	0.673	0.311	0.229	0.304	0.211
AI	56.8	64.1	0.282	0.333	−0.276	0.051	0.296	0.353	−0.065
SVR7	59.5	66.8	0.290	0.339	−0.458	0.020	0.313	0.372	−0.179

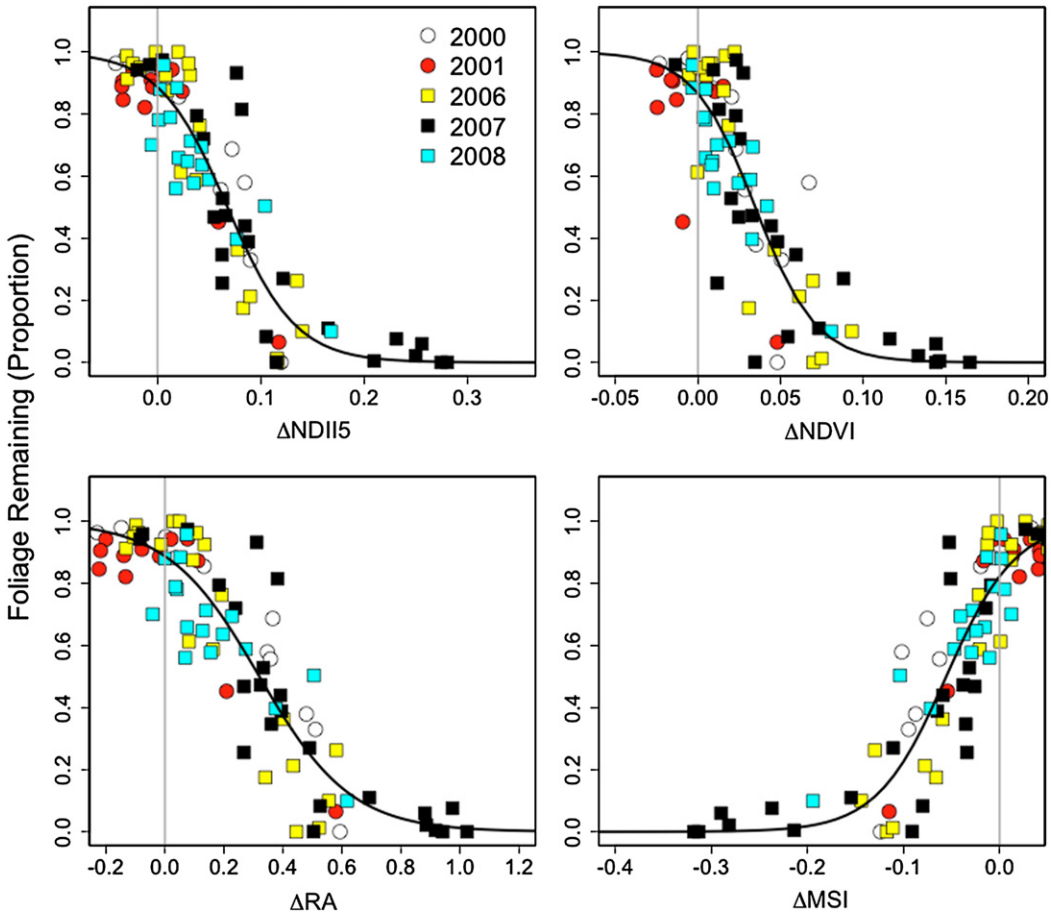

Fig. 3. Model results for vegetation indices to predict gypsy moth defoliation by year and study site (circles = Green Ridge, squares = Savage River). Lines indicate best-fit 2-parameter sigmoidal model as reported in Table 3.

and non-defoliation years. It is also noteworthy that all sites with ΔNDII5 ≤ 0 are clearly not defoliated based on the field data (Fig. 3).

Using RMS error as a metric, the overall model performed best for 2001 (8.2%) and worst for 2007 (17.0%) (Table 5). Although we report CV-R^2 values, these are not the best measures of model performance. For instance, 2008 has a low CV-R^2, but its RMS error is also low (12.8%). This is because this was the last year of the Savage River defoliation, and overall foliage consumption was much lower in 2008 than the other years. The cross-validation results mirror the model results (Fig. 4), indicating a high level of stability in the model even when data from each year is removed. The models developed without each year (Cross-Validation 2 in Table 5) perform uniformly well, providing support for our assertion that the global model we developed is applicable across years, even those without field data for calibration.

We applied the model reported in Table 4 to the sets of images listed in Table 1. The maps of defoliation show distinct patterns associated with the 2000–2001 (Green Ridge, Fig. 5A–B) and 2006–2008 (Savage River, Fig. 5E–G) defoliation events. The defoliation events in 2000–2001 were scattered, with patches of intense defoliation. In 2001, the naturally-occurring fungal pathogen *Entomophaga maimaiga* reduced gypsy moth populations as the larvae matured to their largest and most voracious feeding stages. In Savage River, the defoliation event was widespread and locally intense in 2006, then exploded in 2007 (Fig. 5E–G, see also Fig. 2), before receding again in 2008 when the *Entomaphaga* again reduced the gypsy moth population. Note that areas sprayed for the suppression of gypsy moth in Savage River are clearly evident in Fig. 5E–G as a block in the center right where almost no defoliation is mapped.

We also applied the global model to images of Green Ridge for two years in which very little (2002) or no defoliation (2008) was reported by the Maryland Department of Agriculture (Fig. 5C–D). For 2002, the resulting map (Fig. 5C) shows a few small patches of defoliation, while the map derived for 2008 shows no defoliation. Sketch maps for those years also indicate no gypsy moth activity. Based on these visual comparisons, our model appears to capture

Table 4
Parameter estimates for the fixed-effects ("global") model using ΔNDII5.

Parameter	Estimate	±1 SE	T^{***}
c	2.059	0.305	11.23
d	−30.394	3.275	−11.28

*** $p < 0.0001$ (Nagelkerke's $R^2 = 0.844$, $F_{(3,84)} = 273.16$, n = 84, RMSE = 0.135).

Table 5
Cross-validation results by year.

Year	Global model[a]			Cross-validation 1			Cross-validation 2		
	MAE	RMSE	RSQ	MAE	RMSE	RSQ	MAE	RMSE	RSQ
2000	0.073	0.111	0.871	0.079	0.116	0.859	0.100	0.138	0.840
2001	0.069	0.082	0.898	0.070	0.083	0.896	0.102	0.142	0.828
2006	0.108	0.132	0.876	0.123	0.146	0.848	0.094	0.134	0.835
2007	0.110	0.170	0.769	0.111	0.173	0.762	0.091	0.118	0.849
2008	0.099	0.128	0.589	0.121	0.152	0.423	0.092	0.135	0.866

Cross-validation 1 quantifies how well that year is predicted by model built without that year.
Cross-validation 2 quantifies how well the model that excludes that year performs on all of the data.
[a] Quantifies how well global model fits individual years.

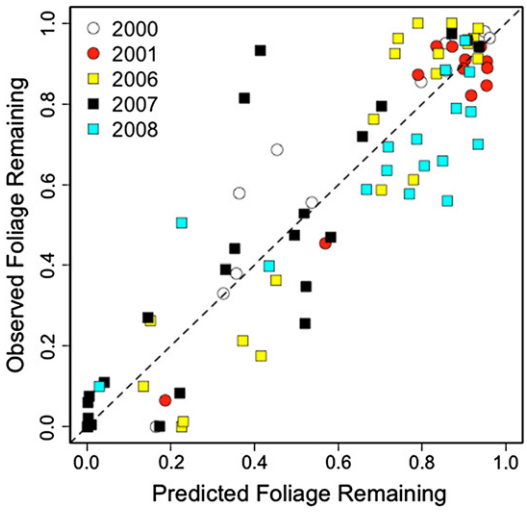

Fig. 4. Results of the cross-validation of the global model (circles = Green Ridge, squares = Savage River). All plots from each year were removed successively and the model rebuilt each time. The predictions on the Y-axis are for the removed plots that were predicted using the model in which that year was removed.

the lack of defoliation disturbance in the observed non-defoliation years.

The only year in which two images capturing a defoliation event were available was 2001, in which we have scenes dated 24 July and 25 August. For the global model, we used the 25 August image because it was cloud-free while the July image had cumulus clouds dotted throughout. Although the July image was timed closer to peak defoliation, the global model exhibited a stronger fit to the field data using the August image as the target defoliation image. The results suggest that in these oak-dominated forests, re-foliation is relatively minor compared to the overall signal of defoliation, especially in dry years such as 2001 and 2007. Indeed, this result is corroborated by an examination of the imagery and maps for Savage River for 2007, also from 25 August (Figs. 2B and 5F). Heavy defoliation is clearly evident in the August 2007 image, despite potential re-foliation, and the error rates for 2007 were reasonable (Table 5). Our testing of the set of alternate base image (25 June 2005 instead of 7 July 2001) for Savage River in 2006–2008 showed little difference, and we conclude that image selection for both target and base images should be optimized to select cloud-free images on the closest available anniversary dates.

The model using growth data indicates that the sigmoidal curves representing defoliation (Fig. 3) can be extended to capture foliar growth as well (Fig. 6). We developed a single model for defoliation and growth using NDII5. For this model, we constrained the inflection point of the curve to zero, such that the crossover from defoliation to regrowth would occur at $\Delta NDII = 0$ (parameter $c = 0$ in Eq. (1)). On the other hand, we have no measure of the potential maximum regrowth, so we modeled the upper asymptote. The resulting model ($F_{(3,108)} = 513.3$, $p < 0.0001$) took the form:

$$\text{Foliage change} = b/(1 + \exp[-d * \Delta NDII]) - 1, \quad (3)$$

where $b = 1.82$ and $d = -15.14$. This indicates an upper asymptote of 82% foliar increase. Model performance was similar to the global model, with a mean absolute error of 0.128 (12.8%), an RMS error of 0.165 and Nagelkerke's $R^2 = 0.86$.

The application of our global model to the defoliation of aspen forests by forest tent caterpillar yielded maps that visually matched observed patterns (Fig. 7). This is important because US Forest Service sketch maps for Minnesota show a single large polygon of the Arrowhead region indicating defoliation, with no detail. However, detailed patterns of defoliation are evident in the Landsat imagery (Fig. 7A–B) and are captured by the map (Fig. 7C). Our approach likely works because both the oak forests of the Appalachians and the aspen forests of Minnesota are closed canopy broadleaf systems, where multispectral response from foliage removal is equivalent. In contrast to Appalachian oak forests, however, aspen forests usually refoliate more readily (i.e. rapidly and completely), meaning that the timing of image acquisition is an important consideration for mapping defoliation of this species. Although there is no way to absolutely validate the assessment of the 2001 aspen defoliation, we provide this example as a demonstration of the possibilities of our approach for retrospective analyses of locations and time period of the Landsat record for which field validation is limited or unavailable.

4. Discussion

We were able to consistently map gypsy moth defoliation using simple differences of NDII5 between defoliation and non-defoliation years across two study sites and five different years. In addition, application of the model to non-defoliation years correctly predicted no defoliation. Cross validation resulted in error estimates of 10–15% defoliation, which is about the same level of uncertainty associated with the defoliation estimates. A fixed-effect "global" model with an asymptote of 1 (no defoliation) and an intercept of 0 (100% defoliation) adequately characterized defoliation across all events, while the results of more complex models with random effects by year yielded no improvement over the global model. The model should be sufficient to map defoliation for other years in our study areas, and probably in other study areas having similar forest characteristics.

The success of our effort depended on having images that were radiometrically comparable. All of the images that we used were from mid-summer (within a 6-week anniversary date span), and were processed to surface reflectance identically. The images were downloaded from USGS at the same time, so the level of processing at USGS was consistent. Prior to the opening of the USGS archive, we had used nearest-neighbor resampled images from the same dates to map defoliation (Townsend et al., 2004), and the results were considerably more noisy. It appears that the cubic-convolution resampled data provided by USGS reduce the effects of misregistration that are prominent in change detection analyses using nearest-neighbor resampling.

Our results suggest that the model for mapping defoliation (Table 4) is extendable to other years and places. A logical next step is to test the robustness of the model with other data from sensors that also measure reflectance in the SWIR and NIR. Likewise, further testing is required to establish that the model is extensible to defoliators other than the gypsy moth, although our results are promising for the forest tent caterpillar. It is likely that coefficients for models of defoliation of evergreen conifers will differ from this work, but we predict that a similar overall modeling approach using ΔNDII5 (Eqs. (1) and (2)) will succeed, with two important caveats: (1) as evergreens, the analyses will have to address cumulative defoliation in addition to current-year defoliation, and (2) the interpretation of the results will be sensitive needle removal (needles are clipped, but not consumed and fall into the canopy) and color change in addition to needle consumption (see Radeloff et al., 1999).

Ultimately, the benefit to our approach is that it is straightforward and: (1) it requires images processed identically to surface reflectance, with (2) one image from a non-defoliation year and one from a defoliation year, and (3) the actual change detection is a simple difference of the two NDII5 images. Our results confirm other studies showing that NIR/SWIR-based indices such as NDII5 are preferred to VIS/NIR indices such as NDVI for mapping defoliation (De Beurs & Townsend, 2008; Fraser & Latifovic, 2005). However, our results (Table 3) indicate that NDVI remains viable for mapping defoliation in absence of suitable SWIR bands. Additional modeling application

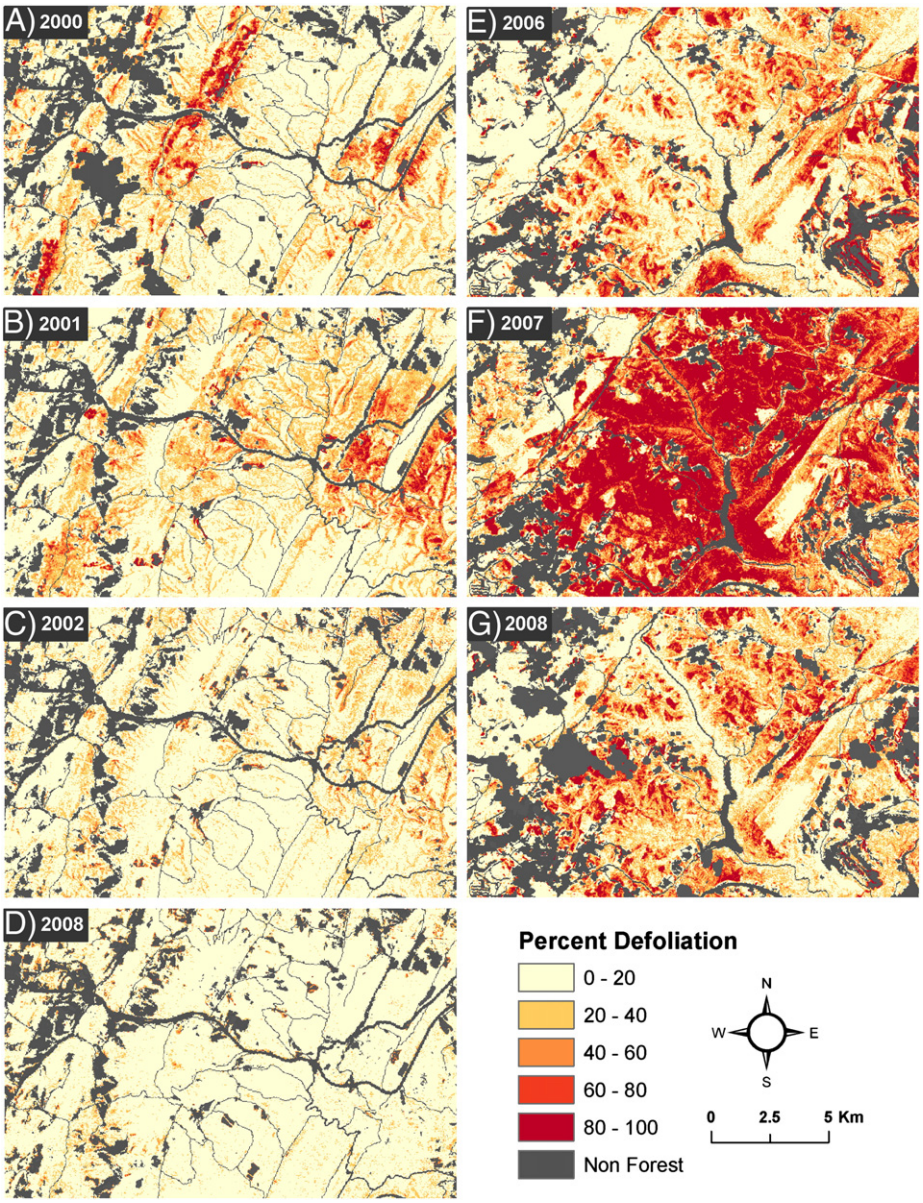

Fig. 5. Maps of percent defoliation by gypsy moth for a subset area of Green Ridge in (A) 2000, (B) 2001, (C) 2002, (D) 2008 and Savage River in (E) 2006, (F) 2007 and (G) 2008. Location of subset areas are shown on Fig. 1. Gray areas indicate non-forest, clouds and cloud shadows. Logged areas are also masked. Compare Savage River results to Landsat images shown in Fig. 2.

and validation studies involving other regions, more extensive field data and insect defoliators are recommended.

Our results are distinguished from other studies in that we map foliage retained (and its inverse, proportion defoliated) as a continuous range from 0 to 100%. Other efforts to map defoliation have produced categorical maps. Even with the estimated ±10–15% error of our maps, we provide information that will be useful to assess the relative spatial variations in impacts of defoliation. Clearly, improvement in spatial predictions of forest growth and productivity, forest watershed nutrient retention, and possibly fire hazards will be valuable for management and recreational purposes. In remote areas with little direct mapping of defoliation disturbance, or in any area lacking resources for intense mapping of insect defoliation, our model, along with suitable Landsat data, will also be useful for identification of areas in need of management prescriptions or for monitoring of forest resource conditions.

Although this study is specific to forest defoliation rather than mortality, our work has actual or potential value for other types of forest disturbance monitoring. For example, there is a considerable literature on the use of multispectral imagery to map mortality due to insects such as the mountain pine beetle. However, most studies tend toward mapping categorical variables rather than producing maps with continuous estimates of damage (e.g., Hatala et al., 2010; Hicke & Logan, 2009; Wulder et al., 2005). Studies that employ hyperspatial data can generate maps of damage rates because of the ability to map individual trees, although at the cost of broad spatial coverage.

One of the strengths of our study is that we had field data to characterize defoliation across five events in two study areas. It is notable that the methods of field data collection varied from year to year, with estimates of defoliation being derived from frass (excrement) collections, allometry, and optical estimates of percent defoliation. Nevertheless, our model produced consistent results across years regardless of the specific field method used for estimating defoliation. This provides additional evidence that the approach is both extensible across studies and robust against differences in measurement and measurement error. We do not suggest that differences in defoliation

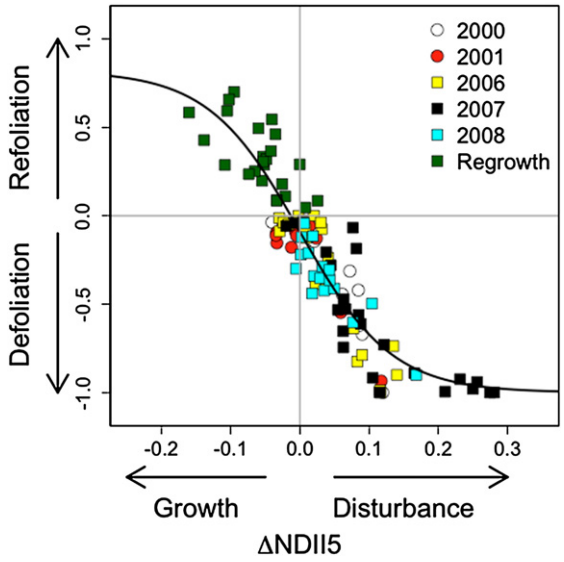

Fig. 6. Model using regrowth estimates to predict growth and defoliation.

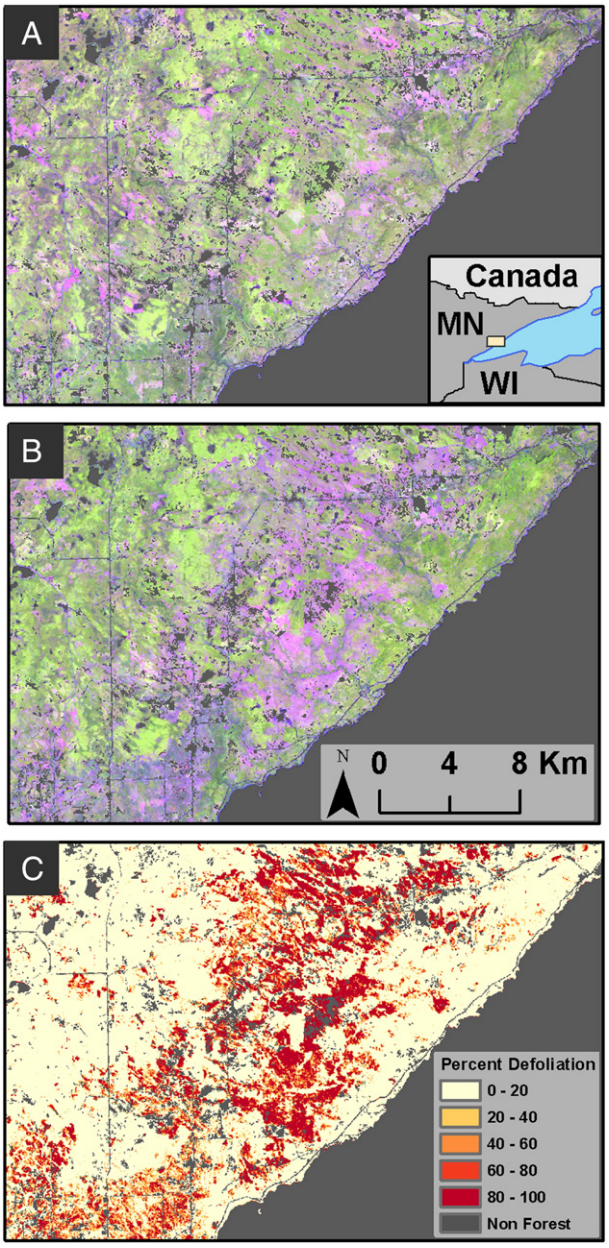

Fig. 7. Defoliation by the forest tent caterpillar in northern Minnesota in 2001: (A) Base image from DD Month 2002, (B) Target defoliation image from DD July 2001, (C) Mapped defoliation using the global model presented in Table 4. Color scheme is same as Figs. 2 and 5.

estimation techniques have no impacts on defoliation predictions. However, we do feel that the robustness of our methods largely overcomes the inherent differences in empirical data collections. Our work does point to the importance of field calibration and validation. Although we used a jack-knife approach for model evaluation, the ideal study would use an independent image data set, for example high resolution imagery timed to peak defoliation, which were not available for this study.

Our approach is based on quantitative assessment of changed in reflectance of defoliated canopies, and appears to work with other defoliator species (forest tent caterpillar in Minnesota aspen forests). We expect that the method would also work across a range of forest types – not just oaks – defoliated by the gypsy moth. Defoliation of conifers by the gypsy moth was not addressed specifically in this study and would require further work to assess the extensibility to forests with different leaf physiognomies. Several of our field plots were of mixed oak–conifer composition and did exhibit bias in the residuals.

Our model of proportion of foliage retained (Eq. (1), Table 4) assumes an asymptote of one, namely that from year-to-year, some forests experience no defoliation. This is the basis for using a model with a sigmoidal form. From a remote sensing perspective, this is borne out by the ΔNDII5 data, in which some areas exhibit negative ΔNDII5, i.e. NDII increases from the base year to the target year, indicating a forest that has greened between years (Eq. (2), see Fig. 3A). Yet it is unusual to measure zero defoliation using field methods, even if a forest is thriving compared to a previous year. Herbivorous insects, including larvae of the gypsy moth, are always present, even if the forest is not undergoing an irruptive, regionally evident defoliation. Our field data from Green Ridge for 2008, a year without major gypsy moth activity, illustrate this. In 2008, average defoliation in plots in which no larvae were observed ($n=15$) was estimated at 13.3%, with a minimum of 6.6%. This means that at the lower end of the predictions (upper end of foliage retained), the maps will always show some level of insect activity. These low levels of defoliation activity do not represent error in the maps, but, depending on the application, users of the maps may want to adjust the predicted range to capture the effective range of foliage removed/retained. By definition field measures provide within-year estimates of defoliation as [foliage removed (in yr x)]/[foliage produced (in yr x)]. In contrast, ΔVI characterizes defoliation as a between-year difference, i.e. [foliage removed (in yr x)]/[foliage produced (in yr a)], where year a is a base year. The field data effectively biases the model asymptote away from 1 since there is no measure of defoliation in the base year. Because defoliation is a relative measure, non-defoliation years are expected to exhibit foliage retention of ≥ 1, i.e. increasing leaf area. We show that the sigmoidal curve (Fig. 2) can be extended to capture regrowth (Fig. 6) and potentially provide a better representation of overall canopy foliage disturbance and recovery. Full implementation of the disturbance/growth model would require dedicated sampling of year-to-year foliage dynamics in non-disturbed years.

The choices of base and target (defoliation) images are also important to the broader application of our approach. In our study, we used defoliation images that ranged in date from 19 July to 25 August. Depending on weather, gypsy moth population levels, suppression efforts, and pathogens such as *E. maimaiga*, peak defoliation in the study area may occur any time between late June and mid-July,

with potential re-foliation occurring up to a month later. This makes for a highly dynamic and variable system from year to year. Model error between and within years (Figs. 2 and 4) can likely be attributed to some of these factors. However, our results indicate that the method is relatively robust across a range of dates. Indeed the results do confirm the observation that even when forests re-foliate, it is likely proportional to defoliation, and, at least in Central Appalachian oak forests, of limited signal in the Landsat images. It may be that other satellites or planned sensors with superior radiometric resolution and signal-to-noise than Landsat 5 and Landsat 7 will be more sensitive to re-foliation response.

For this study, we selected base images from years that were as few years as possible previous to the defoliation years, were cloud-free and for which no defoliation had been reported, although this does not guarantee that no defoliation occurred. This meant a time difference of one and two years for the 2000–2001 Green Ridge defoliations, and 5+ years for the Savage River outbreaks. Although we are not aware of any issues with the 2001 base image for Savage River, we did have to exclude four plots from our analysis in Green Ridge because the sites experienced a walking stick defoliation in the base year, 1999. We were fortunate to have this information from a different study that sampled these field sites in 1999. However, it is altogether plausible that isolated defoliation or other canopy disturbances occurred elsewhere in our Landsat scenes. Discrimination of defoliation from other disturbances (e.g. logging, other defoliators) is also important to the interpretation of results from this model. Ultimately, the identification of undisturbed base images is important to this approach, but given a long enough time-series of Landsat TM/ETM+ and future data sets, we will be able to develop pixel-wise base maps of maximum greenness using data across multiple years rather than a single base image (e.g., Spruce et al., 2011; Deel et al., accepted for publication).

Our results are encouraging in light of the potential launch of Landsat data continuity mission. The strength of our results in light of the diminished SNR of late-era Landsat 5 imagery suggests that the signal of defoliation in broadleaf forests is strong, and that the relationships are stable. The next steps include testing our approach for mapping disturbance in additional systems, and applying the results to past events, such as gypsy moth defoliation from the 1980s.

5. Conclusion

We have presented a straightforward method to estimate defoliation using Landsat imagery with radiometric, atmospheric, and topographic corrections. Ultimately, we conclude that our approach should be suitable both for characterizing future defoliation events, as well as back-casting defoliation events – with limitations – in the recent historical record. If implemented as a monitoring strategy, a small, but careful effort of field monitoring should provide the necessary data to refine, update and validate the model parameters. Key considerations of the applicability of our model include composition of the defoliated species and vegetation phenology of pre- and post-defoliation images. With improved sensors and image data, the capacity to detect defoliation will only improve. From an ecological perspective, our approach allows characterization of a forest disturbance process that significantly impacts above- and below-ground forest productivity, as well as nutrient dynamics (e.g., see McNeil et al., 2007; Townsend et al., 2004). This research may be especially useful in landscape-scale carbon modeling, where the characterization of disturbances is a key uncertainty (Hicke et al. 2012).

Acknowledgments

The research and data presented in this paper was supported by funds from a number of grants dating to 1999. Primary funding for this research was provided by NASA Interdisciplinary Sciences Grant NNG04GL87G to PAT and KNE and NASA Carbon Cycle Science Grant NNX06AD45G to PAT. Additional funding supporting the collection of data presented in this paper include EPA Ecological Indicators STAR grant R826598 to SWS and PAT (2000 defoliation data) and NSF SGER grant DEB-0119581 to KNE and PAT (2001 defoliation data). Data analyses were also supported by US Forest Service Special Technology Development Program (STDP) grant 09-CA-11420004-021 to PAT. Numerous people were involved in the collection and analysis of the field data used in this study. In particular, we would like to express our appreciation to Brian Sturtevant, Robert Chastain, Jeremiah Sawma, Wendy Hunter, Michael Snyder, James Morgan, and Jeff Griffith. This research is also the result of innumerable discussions among the researchers at the Appalachian Laboratory and University of Wisconsin. We also thank Clay Baros, Kirsten de Beurs, Shawn Serbin, Brenden McNeil and Suming Jin for their intellectual contributions to this work. We gratefully acknowledge the helpful comments of three anonymous reviewers. None of the research or data presented in this paper has been published previously.

References

Arzani, H., & King, G. W. (1997). Application of remote sensing (Landsat TM data) for vegetation parameters measurement in western division of NSW. *Proceedings XVIII IGC 1997 Winnepeg, Manitoba*. Accessed from www.internationalgrasslands.org/publications/pdfs/1997/2_21_019.PDF.

Burnham, K. P., & Anderson, D. R. (2002). *Model selection and multimodel inference: A practical information–theoretic approach* (2nd ed.). Springer-Verlag.

Ciesla, W. M., Dull, C. W., & Acciavatti, R. E. (1989). Interpretation of SPOT-1 color composites for mapping defoliation of hardwood forests by gypsy moth. *Photogrammetric Engineering and Remote Sensing*, *55*, 1465–1470.

Conway, B. E., McCullough, D. G., & Leefers, L. A. (1999). Long-term effects of jack pine budworm outbreaks on the growth of jack pine trees in Michigan. *Canadian Journal of Forest Research*, *29*, 1510–1517.

Cox, D. R., & Snell, E. J. (1989). *The analysis of binary data* (Second ed.). London: Chapman and Hall.

Crist, E. P., & Kauth, R. J. (1986). The tasseled cap de-mystified. *Photogrammetric Engineering and Remote Sensing*, *52*(1), 81–86.

Dale, V. H., Joyce, L. A., McNulty, S., Neilson, R. P., Ayres, M. P., Flannigan, M. D., et al. (2001). Climate change and forest disturbances. *Bioscience*, *51*, 723–734.

De Beurs, K. M., & Townsend, P. A. (2008). Estimating the effect of gypsy moth defoliation using MODIS. *Remote Sensing of Environment*, *112*, 3983–3990.

Deel, L.N., McNeil, B.E., Serbin, S.P., Singh, A., Curtis, P.G., Eshleman, K.N., & Townsend, P.A. (in press). Relationship of a Landsat cumulative disturbance index to canopy nitrogen and forest structure. Remote Sensing of Environment.

Eklundh, L., Johansson, T., & Solberg, S. (2009). Mapping insect defoliation in Scots pine with MODIS time-series data. *Remote Sensing of Environment*, *113*, 1566–1573.

Elvidge, C. D., & Lyon, R. J. P. (1985). Estimation of the vegetation contribution to the 1.65/2.22 mm ratio in air-borne thematic-mapper imagery of the Virginia Range, Nevada. *International Journal of Remote Sensing*, *6*, 75–88.

Eshleman, K. N., McNeil, B. E., & Townsend, P. A. (2009). Validation of a remote-sensing based index of forest disturbance using streamwater nitrogen data. *Ecological Indicators*, *9*, 476–484.

Eshleman, K. N., Morgan, R. P., II, Webb, J. R., Deviney, F. A., & Galloway, J. N. (1998). Temporal patterns of nitrogen leakage from mid-Appalachian forested watersheds: Role of insect defoliation. *Water Resources Research*, *34*, 2017–2030.

Fajvan, M. A., & Wood, M. J. (1996). Stand structure and development after gypsy moth defoliation in the Appalachian Plateau. *Forest Ecology and Management*, *89*, 79–88.

Franklin, S. E., Fan, H., & Guo, X. (2008). Relationship between Landsat TM and SPOT vegetation indices and cumulative spruce budworm defoliation. *International Journal of Remote Sensing*, *29*, 1215–1220.

Fraser, R. H., & Latifovic, R. (2005). Mapping insect-induced tree defoliation and mortality using coarse spatial resolution imagery. *International Journal of Remote Sensing*, *26*, 193–200.

Hall, R. J., Fernandes, R. A., Hogg, E. H., Brandt, J. P., Butson, C., Case, B. S., et al. (2003). Relating aspen defoliation to changes in leaf area derived from field and satellite remote sensing data. *Canadian Journal of Remote Sensing*, *29*, 299–313.

Hardisky, M. A., Klemas, V., & Smart, R. M. (1983). The influence of soil salinity, growth form, and leaf moisture on the spectral reflectances of *Spartina alterniflora* canopies. *Photogrammetric Engineering and Remote Sensing*, *49*, 77–83.

Hatala, J. A., Crabtree, R. L., Halligan, K. Q., & Moorcroft, P. R. (2010). Landscape-scale patterns of forest pest and pathogen damage in the Greater Yellowstone Ecosystem. *Remote Sensing of Environment*, *114*, 375–384.

Healy, S. P., Cohen, W. B., Zhiqiang, Y., & Krankina, O. N. (2005). Comparison of tasseled cap-based Landsat data structures for use in forest disturbance detection. *Remote Sensing of Environment*, *97*.

Hicke, J. A., Allen, C. D., Desai, A. R., Dietze, M. C., Hall, R. J., Hogg, E. H., et al. (2012). Effects of biotic disturbances on forest carbon cycling in the United States and Canada. *Global Change Biology*, *18*, 7–34, doi:10.1111/j.1365-2486.2011.02543.x.

Hicke, J. A., & Logan, J. (2009). Mapping whitebark pine mortality caused by a mountain pine beetle outbreak with high spatial resolution satellite imagery. *International Journal of Remote Sensing*, *30*, 4427–4441.
Huete, A., Didan, K., Miura, T., Rodriguez, E. P., Gao, X., & Ferreira, L. G. (2002). Overview of the radiometric and biophysical performance of the MODIS vegetation indices. *Remote Sensing of Environment*, *83*, 195–213.
Hunt, E. R., & Rock, B. N. (1989). Detection of changes in leaf water content using near and middle-infrared reflectances. *Remote Sensing of Environment*, *30*, 43–54.
Hurley, A., Watts, D., Burke, B., & Richards, C. (2004). Indentifying gypsy moth defoliation in Ohio using Landsat data. *Environmental and Engineering Geoscience*, 321–328.
Jenkins, J. C., Chojnacky, D. C., Heath, L. S., & Birdsey, R. A. (2003). National-scale biomass estimators for United States tree species. *Forest Science*, *49*(1), 12–35.
Jepsen, J. U., Hagen, S. B., Hogda, K. A., Ims, R. A., Karlsen, S. R., Tommervik, H., et al. (2009). Monitoring the spatio-temporal dynamics of geometrid moth outbreaks in birch forest using MODIS–NDVI data. *Remote Sensing of Environment*, *113*, 1939–1947.
Jin, S., & Sader, S. A. (2005). Comparison of time-series tasseled cap wetness and the normalized difference moisture index in detecting forest disturbances. *Remote Sensing of Environment*, *94*, 364–372.
Johnson, E. W., & Ross, J. (2008). Quantifying error in aerial survey data. *Australian Forestry*, *71*, 216–222.
Jordan, C. F. (1969). Derivation of leaf area index from quality of light on the forest floor. *Ecology*, *50*, 663–666.
Joria, P. E., & Ahearn, S. C. (1991). A comparison of the SPOT and Landsat Thematic Mapper satellite systems for detecting gypsy moth defoliation in Michigan. *Photogrammetric Engineering and Remote Sensing*, *57*, 1605–1612.
Katovich, S., & Hanson, J. (2001). *Forest tent caterpillar in the upper Midwest. Information Sheet NA-PR-02-01*. Newtown Square, PA: U.S. Dept. of Agriculture, Forest Service, Northern Area State & Private Forestry.
Kotchenova, S. Y., Vermote, E. F., Matarrese, R., & Klemm, F. (2006). Validation of a new vector version of the 6S radiative transfer code for atmospheric correction of MODIS data: Part I — Path radiance. *Applied Optics*, *45*(26), 6762–6774.
MacLean, D. A., & MacKinnon, W. E. (1996). Accuracy of aerial sketch-mapping estimates of spruce budworm defoliation in New Brunswick. *Canadian Journal of Forest Research*, *26*, 2099–2108.
Man, G. (2010). Major forest insect and disease conditions in the United States: 2009 update. *USDA Forest Service report FS-952*.
Masek, J. G., Vermote, E. F., Saleous, N. E., Wolfe, R., Hall, F. G., Huemmrich, K. F., et al. (2006). A Landsat surface reflectance dataset for North America, 1990–2000. *IEEE Geoscience and Remote Sensing Letters*, *3*, 68–72.
McNeil, B. E., de Beurs, K. M., Eshleman, K. N., Foster, J. R., & Townsend, P. A. (2007). Maintenance of ecosystem nitrogen limitation by ephemeral forest disturbance: An assessment using MODIS, Hyperion, and Landsat ETM. *Geophysical Research Letters*, *34*, L19406.
Moskal, L. M., & Franklin, S. E. (2004). Relationship between airborne multispectral image texture and aspen defoliation. *International Journal of Remote Sensing*, *25*, 2701–2711.
Muchoney, D. M., & Haack, B. N. (1994). Change detection for monitoring forest defoliation. *Photogrammetric Engineering and Remote Sensing*, *60*, 1243–1251.
Muzika, R. M., & Liebhold, A. M. (1999). Changes in radial increment of host and non-host tree species with gypsy moth defoliation. *Canadian Journal of Forest Research*, *29*, 1365–1373.
Nagelkerke, N. J. D. (1991). A note on a general definition of the coefficient of determination. *Biometrika*, *78*, 691–692.
Naidoo, R., & Lechowicz, M. J. (2001). Effects of gypsy moth on radial growth of deciduous trees. *Forest Science*, *47*, 338–348.
Radeloff, V. C., Mladenoff, D. J., & Boyce, M. S. (1999). Detecting Jack Pine budworm defoliation using spectral mixture analysis: Separating effects from determinants. *Remote Sensing of Environment*, *69*, 156–169.
Rock, B. N., Vogelmann, J. E., Williams, D. L., Vogelmann, A. F., & Hoshizaki, T. (1986). Remote detection of forest damage. *BioScience*, *36*(7), 439–445.
Royle, D. D., & Lathrop, R. G. (1997). Monitoring hemlock forest health in New Jersey using Landsat TM data and change detection techniques. *Forest Science*, *43*, 327–335.
Spruce, J. P., Sader, S., Ruan, R. E., Smoot, J., Kuper, P., Ross, K., et al. (2011). Assessment of MODIS NDVI time series data products for detecting forest defoliation by gypsy moth outbreaks. *Remote Sensing of Environment*, *115*, 427–437.
Swank, W. T., Waide, J. B., Crossley, D. A., & Todd, R. L. (1981). Insect defoliation enhances nitrate export from forest ecosystems. *Oecologia*, *51*, 297–299.
Teillet, P. M., Guindon, B., & Goodenough, D. G. (1982). On the slope-aspect correction of multispectral scanner data. *Canadian Journal of Remote Sensing*, *8*, 84–106.
Townsend, P. A. (2001). Relationships between vegetation patterns and hydroperiod on the Roanoke River floodplain, North Carolina. *Plant Ecology*, *156*, 43–58.
Townsend, P. A., Eshleman, K. N., & Welcker, C. (2004). Remote estimation of gypsy moth defoliation to assess variations in stream nitrogen concentrations. *Ecological Applications*, *14*, 504–516.
Tucker, C. J. (1979). Red and photographic infrared linear combinations for monitoring vegetation. *Remote Sensing of Environment*, *8*, 127–150.
Vogelmann, J. E., & Rock, B. N. (1989). Use of Thematic Mapper data for the detection of forest damage caused by the Pear Thrips. *Remote Sensing of Environment*, *30*, 217–225.
Williams, D. L., Nelson, R. F., & Dottavio, C. L. (1985). A georeferenced LANDSAT digital database for forest insect-damage assessment. *International Journal of Remote Sensing*, *6*, 643–656.
Wolter, P. T., & Townsend, P. A. (2011). Estimating forest composition and structure using multi-temporal/multi-sensor image data in a PLS framework. *Remote Sensing of Environment*, *115*, 671–691, doi:10.1016/j.rse.2010.10.010.
Wolter, P. T., Townsend, P. A., Kingdon, C. C., & Sturtevant, B. R. (2008). Remote sensing of the distribution and abundance of host species for spruce budworm in northern Minnesota and Ontario. *Remote Sensing of Environment*, *112*, 3971–3982.
Wulder, M. A., Skakun, R. S., Dymond, C. C., Kurz, W. A., & White, J. C. (2005). Characterization of the diminishing accuracy in detecting forest insect damage over time. *Canadian Journal of Remote Sensing*, *31*, 421–431.